Appl Phys A (2013) 113:981–988
DOI 10.1007/s00339-013-7726-z

Applied Physics A
Materials Science & Processing

Chemical corrosion by chlorides on ancient-like bronzes and treatment by hydrogen glow discharge plasma

O. Papadopoulou · J. Novakovic · P. Vassiliou · E. Filippaki · Y. Bassiakos

Received: 14 April 2013 / Accepted: 19 April 2013 / Published online: 8 May 2013

Abstract Three representative ancient-like bronzes are employed for the chemical synthesis of $Cu_2(OH)_3Cl$ rich patinas in order to study the influence of the alloying elements in the evolution of the chloride attack and to further conduct stabilization treatment via Hydrogen Glow Discharge Plasma (HGDP) at low temperature and pressure. The corrosion behavior of specimens having Sn and Pb as main alloying elements is governed by a decuprification mechanism and by the formation of Sn–Pb–O enriched barrier layers. In the case of the Zn containing alloy, dezincification is more pronounced at the corrosion initial stages, and copper species predominate the corrosion products evolution. A three-hour HGDP treatment leads to Cu^+ production and metallic Cu, Sn, Zn, and Pb redeposition, as a result of metal cation reduction. This process is accompanied by partial removal of Cl species, O diminution, and change in coloration. The further increase of the Cl/O atomic ratio measured on the post-treated surfaces leads to the formation of nantokite and thus to the conclusion that the stabilization of objects with extensive Cl attack is not feasible by HGDP without preliminary chemical treatment.

1 Introduction

Copper alloys, depending on the corrosive environment, may exhibit a variety of corrosion products. The most aggressive environments are those rich in chlorine species due to the instability that their presence imparts to the metallic surface. Thus, the removal of these species from the surface of bronze artefacts is very important in order to inhibit a self-accelerated corrosion process known as "bronze disease" [1, 2]. It is not only the chemical composition of an alloy that affects both the corrosion profile and the cleaning treatment efficiency; different metallurgical characteristics such as the composition and size of dendritic formations can create microgalvanic phenomena during the corrosion process [3–6]. Thus surfaces of extensive heterogeneity are produced, which greatly complicate every effort to understand how these "subsystems" contribute to the overall corrosion mechanism and to apply a suitable stabilization treatment. Although there is a considerable number of chemical treatments for the conservation of copper, bronze, and brass, most are not satisfactory for cupreous metals recovered from marine sites [7]. Taking into account effectiveness and what patination changes are acceptable, traditional methods exhibit many disadvantages as conservation techniques are frequently very laborious, and if chemical treatments are used to replace intricate manual work, it is difficult to ensure sufficient control and selectivity.

The reduction of corrosion layers using Hydrogen Glow Discharge Plasma (HGDP) is considered as a novel technique compared to the traditional cleaning treatments applied on copper alloys, although its initial application to metals conservation dates back to 1979 [8–15]. The method is based on the reduction of the corrosion products, at low pressure and temperature, by chemically reactive species such as ions and radicals, which are produced in electrical discharges with the use of a gas or a mixture of gases.

This work consists of two parts. The first is the chemical synthesis of a corrosion stratification containing the main corrosion products encountered on bronze objects severely

O. Papadopoulou (✉) · J. Novakovic · P. Vassiliou
School of Chemical Engineering, National Technical University of Athens, 9 Iroon Polytechniou Str., 15780 Athens, Greece
e-mail: olpap@central.ntua.gr

E. Filippaki · Y. Bassiakos
Laboratory of Plasma Physics, Institute of Materials Science, NCSR 'Demokritos', Athens, Greece

attacked by chlorine species. Three representative ancient-like cast bronzes (one rich in Sn, one rich in Zn, and one rich in Pb) were employed as substrates in order to study the influence of the alloying elements in the evolution of corrosion. For the second part, these corroded specimens were further treated by HGDP in order to further investigate the potentials of this method as a stabilization treatment on heavily attacked surfaces with active "bronze disease."

2 Experimental

2.1 Bronze alloys

The three cast bronzes are: a typical binary bronze having Pb as trace element (TB–Cu 92.3, Sn 7.5, Pb 0.2 %w/w), a ternary leaded bronze (LB–Cu 88.0, Sn 4.0, Pb 8.0 %w/w) and a quaternary zincian bronze (ZB–Cu 82.5, Zn 14.0, Sn 3.0, Pb 0.5 %w/w). As a result of the particular casting conditions employed [16] and the addition of microinclusions (such as copper and copper–iron sulphides), there were produced alloys having microchemical structure and metallurgical features similar to those of ancient alloys. The dimensions of the coin resembling specimens are 26 mm in diameter and 3 mm in height.

2.2 Sample preparation

The specimen surfaces were polished with abrasive papers (up to 1500 grit), degreased by acetone, and rinsed with deionized water. The chemical corrosion process consisted of two stages. In the first stage each specimen was immersed in an 1 M $CuCl_{2(aq)}$ solution, sealed from the atmosphere, for a period of 72 h. In the second stage specimens were sealed in a container in 100 % relative humidity (%RH) for an incubating period of 72 h that led to the formation $Cu_2(OH)_3Cl$, which is typically related to "bronze disease." Between the two stages and after the second stage, the specimens remained in an oven at 80 °C for 24 h, and kept at low %RH conditions.

2.3 Plasma treatment

A radio frequency (RF) glow discharge plasma apparatus, similar to the Veprek's prototype [9], was used. The reactor is a Pyrex-glass bell jar of 40 cm ID and 46 cm length. It is evacuated down to 10^{-2} Torr, and H_2 gas is introduced to the reactor through a needle valve equipped with a flow meter. The temperature is monitored by a thermocouple inserted along the discharge axis in a Pyrex-glass sleeve. The samples are placed on Pyrex grids along the axis of the discharge. Treatment conditions are presented in Table 1.

Table 1 Experimental parameters of HGDP treatment

Gas	Power (kW)	Pressure (Torr)	Temperature (°C)	Duration (h)
100 % H_2	2	0.90	200	3

2.4 Analysis and characterization

Morphology observations and elemental analysis of the corrosion layers at every experimental stage were performed by Scanning Electron Microscopy (SEM) coupled with Energy Dispersive Spectrometry (EDS), using a FEI Quanta 200 scanning electron microscope equipped with a tungsten filament. The accelerating voltage of the incident electron beam was set between 20 and 25 kV. The crystalline compounds on corroded and plasma-treated surfaces were identified by X-Ray Diffraction (XRD), using a SIEMENS 5000 diffractometer, equipped with a Cu Kα X-ray source. The assignment of the crystalline phases was based on the JPDS powder diffraction file cards. All the distinct areas of the corrosion stratification and the cleaned surfaces were documented by means of digital macrophotography.

3 Results and discussion

3.1 Characterization after the immersion in $CuCl_2$ solution

After the first stage of the chemically induced corrosion, wash and exposure to atmospheric air while drying, Sn- and Zn-bronze (TB_1 and ZB_1) were covered with macroscopically similar patinas consisting of a white layer with yellowish areas and some precipitated brown agglomerates adhered on the surface. Pb-bronze (LB_1) was covered with a uniform smooth white and relatively thinner corrosion layer (Fig. 1).

On specimen TB1 backscattered electron imaging reveals the heterogeneity of the crust (Fig. 2a). Local accumulation of Cu compounds and Sn/Pb rich areas can be distinguished as well as a cracking pattern. On ZB_1 the surface is covered by angular, well-crystallized grains, which at higher magnifications appear to be porous. Unlike the other specimens, a spatial segregation of the alloying elements is not observed. On specimen LB_1, the thin corrosion film appears to have an "etching" effect, which highlights the dendritic structure of the alloy matrix as areas rich in Pb and Sn have a whitish appearance. The dendritic structure of the alloy is revealed since the corrosion layer formed after chemical attack is very thin and probably produced by an epitaxial growth mechanism.

The formation of these patinas is the result of a complex mechanism of interrelated redox reactions. Solution concentration, pH, and the relative concentrations of $CuCl_2^0$,

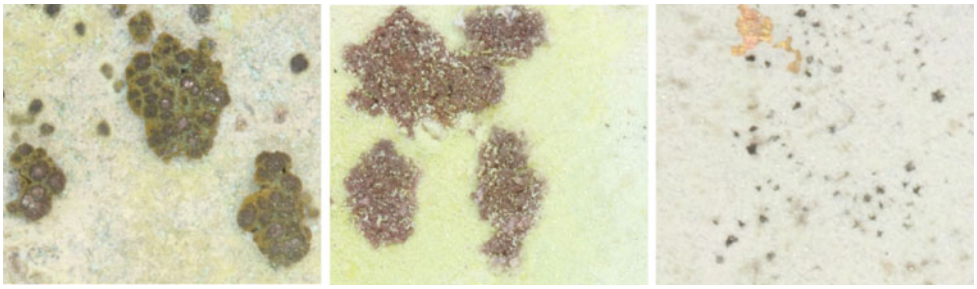

Fig. 1 Photographic documentation of the three bronzes after the immersion in aqueous $CuCl_2$ solution for 72 h and drying: (**a**) TB_1, (**b**) ZB_1, and (**c**) LB_1

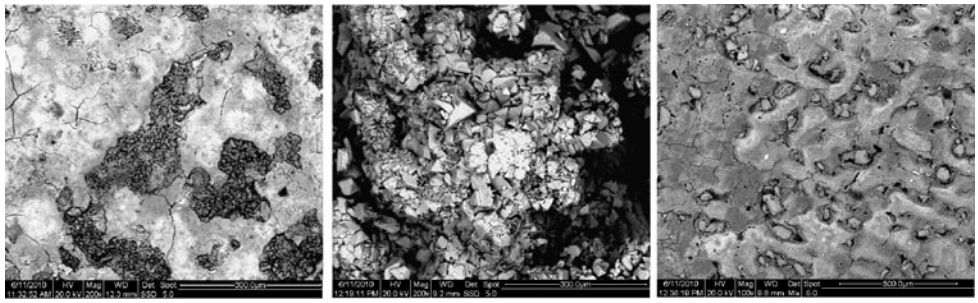

Fig. 2 SEM images of (**a**) TB_1, (**b**) ZB_1, and (**c**) LB_1 revealing the elemental distribution and morphology of the rough surfaces encountered on the three bronzes after the first stage of chemical attack in the $CuCl_2$ solution

$CuCl^+$, $CuCl_4^{2-}$, and $CuCl_2^-$ species are the most important parameters that define the nature of the corrosion products [17]. On the alloy surface, multiple redox couples between the alloying elements are established. It is difficult to predict the chemical state of the corrosion compounds, but the presence of Cu(I), Pb(II) chloride compounds, and Sn(IV) and Sn(II) oxy-hydroxychlorides is expected to be found. On the other hand, Zn chloride compounds are highly soluble in water and therefore unlikely to stay adhered on the surface during immersion. Slow precipitation results in the formation of crystalline solids, while fast precipitation produces poorly crystalline solids, which are difficult to identify by XRD reflections. In the case under examination, the rapid chemical attack in an acidic solution (3.1 pH) does not allow all compounds to crystallize under equilibrium conditions. This is particularly important for the compounds that are believed to form first and contribute to a partial surface passivation—i.e. Sn and Pb compounds—which tend to be nanocrystalline or amorphous. According to [18], passive films generally form as bilayers, with a highly disordered "barrier" layer adjacent to the metal and an outer film comprised of a precipitated phase that may incorporate anions and/or cations from the solution. Because passivity still is observed in the absence of the outer film (e.g., in highly acidic where precipitation may not occur), "passivity" is attributed to the barrier layer. During film growth, cation vacancies are produced at the metal/layer interface but are consumed at the layer/solution interface. Macdonald et al. [19] developed a theory for steady-state passive layers on metals and alloys in aqueous environments, which presents two possibilities after the barrier film formation. If dissolution at the layer-solution interface occurs very slowly, the primary passive film is envisaged to consist of a rigid oxide sublattice that transmits cations from the metal to a gel-like, precipitated upper layer. If dissolution at the barrier film/environment interface occurs rapidly, then a steady-state thickness is achieved by a balance between the rate of dissolution of the layer at the layer-solution interface and the rate of growth of the film into the underlying metal phase, due to the outward movement of the O vacancies (i.e., inward movement of O^{2-}) through the barrier layer. It is assumed that in this experiment, the first hypothesis seems more realistic for the Sn- and Pb-bronze.

The crystalline compounds on TB1 specimen, as identified by XRD, are: CuCl (nantokite), $Pb_2O(CO_3)Cl_2$ (shanonnite), and PbO (lithargite), while on specimen ZB_1 only CuCl is detected. Some of the brown agglomerates were also removed, analyzed by XRD, and identified as metallic Cu, most probably redeposited from the solution. From the LB_1 XRD reflections, the peak assignment corresponds to nantokite (CuCl), cotunite ($PbCl_2$), abhurite ($Sn_{21}Cl_{16}(OH)_{14}O_6$), cerussite ($PbCO_3$), and clinoatacamite. XRD reflections are not presented for reasons of brevity.

The elemental composition of the corroded surfaces is given in Table 2. TB_1 patina EDS analysis testifies to Cu dissolution and a huge enrichment in Sn (having an atomic percentage of 25.1 % Sn with regard to total metal atoms, while the initial Sn concentration in the base metal being only 4.1 %) (Table 3). The Zn-bronze seems to undergo dezincification upon its immersion in the solution, since the Zn atomic percentage drops from 13.9 % to 3.7 % while Sn has

Table 2 Atomic concentration (%) of the elements detected on the corroded and treated surfaces through EDS—bulk and spot—analysis

	Analyzed area	**O**	Cl	**C**	Cu	Sn	Zn	Pb
After 1st and 2nd stage of corrosion	TB_1	40.8	16.3	13.4	21.9	7.4	–	0.2
	TB_2	55.1	17.4		27.5	–	–	–
	ZB_1	16.0	41.0	–	40.4	1.0	1.6	–
	ZB_2	57.2	15.5		27.3			
	LB_1	47.2	10.9	15.2	10.7	11.1	–	4.9
	LB_{2L1}	54.1	18.1	–	23.5	1.4	–	2.9
	LB_{2L2}	52.2	19.9	–	27.2	–	–	0.7
	LB_{2L3}	56.3	16.2	–	27.5	–	–	–
After 3 h HGDP treatment	TB_2	1.9	5.0		92.8	0.3	–	–
	ZB_2	3.0	3.0	–	84.5	0.6	8.9	–
	LB_{2L1}	10.7	1.2		85.9	1.0	–	1.2
	LB_{2L2}	51.1	12.3		31.4	2.3	–	2.9
	LB_{2L3}	15.2	11.1	–	72.5	0.3	–	0.9

Table 3 Calculated values of atomic percentages derived from EDS analyses

Analyzed area	Atomic percentages (%)			
	Cu/total metals	Sn/total metals	Pb/total metals	Zn/total metals
TB-base metal	95.8	4.1	0.1	
TB_1	74.3	25.1	0.6	
TB_2	100	–	–	
TB_2 (HGDP)	99.7	0.3	–	
ZB-base metal	84.1	1.8	0.2	13.9
ZB_1	94.0	2.3	–	3.7
ZB_{2L1}	78.4	4.3	0.4	16.9
ZB_{2L2}	100	–	–	–
ZB_2 (HGDP)	89.9	0.6	–	9.5
LB-base metal	95.0	2.3	2.7	
LB_1	40.2	41.6	18.2	
LB_{2L1}	84.5	5.1	10.4	
LB_{2L2}	97.7	–	2.3	
LB_{2L3}	100	–	–	
LB_{2L1} (HGDP)	97.6	1.1	1.3	
LB_{2L2} (HGDP)	85.8	6.3	7.9	
LB_{2L3} (HGDP)	98.2	0.5	1.3	

a minor enrichment (Table 3). On the Pb-bronze specimen, a vast enrichment in Sn (41.6 % from 2.3 %) and a huge enrichment in Pb (18.2 % from 2.7 %) are indicative of the intense migration of copper outward while only a proportion precipitates on the surface in the form of nantokite (CuCl). LB_1 patina is regarded as the most stable since it is highly enriched in O (47.3 %) and has the smaller percentage of Cl (Table 2), TB_1 follows with 40.7 % O and elevated Cl content, but ZB_1 corrosion layer consists almost entirely of CuCl—the atomic ratio of Cu to Cl is approximately 1:1 (Table 2)—and the concentration of oxygen is low. The remarkable concentration of C in the corrosion layer of TB_1 and LB_1 is a very interesting finding, which confirms the formation of copper and lead carbonates after the removal from the solution and definitely enhances the patinas stability. Taking into account the above analysis and ΔG values [20], the possible reactions ($\Delta G < 0$) that are believed to have taken place at room temperature during the first stage of the implemented corrosion protocol are given below:

during immersion in $CuCl_2$ solution

$$Cu + CuCl_{2(aq)} \rightarrow 2CuCl_{(s)}$$

$$Sn + 2CuCl_{2(aq)} \rightarrow xSnCl_{2(aq)} + (1-x)SnCl_{2(s)} + 2CuCl_{(s)}$$

$$21Sn^{2+}{}_{(aq)} + 16Cl^{-}_{(aq)} + 20H_2O_{(l)} \leftrightarrow Sn_{21}Cl_{16}(OH)_{14}O_{6(s)} + 26H^{+}{}_{(aq)}$$

$$SnCl_{2(s)} + CuCl_{2(aq)} \rightarrow Cu^{0}_{(s)} + SnCl_{4(s)}$$

$$Zn + 2CuCl_{2(aq)} \rightarrow ZnCl_{2(aq)} + 2CuCl$$

$$ZnCl_{2(aq)} + H_2O_{(l)} \rightarrow Zn(OH)Cl_{(s)} + HCl_{(aq)}$$

$$Zn + CuCl_{2(aq)} \rightarrow ZnCl_{2(aq)} + Cu_{(s)}$$

$$Pb_{(s)} + 2CuCl_{2(aq)} \rightarrow PbCl_{2(s)} + 2CuCl_{(s)}$$

after the removal from the solution and exposure to humid atmospheric air

$$PbCl_{2(s)} + H_2O_{(g)} \rightarrow PbO_{(s)} + 2HCl_{(g)}$$

$$CO_{2(g)} + H_2O_{(g)} \leftrightarrow HCO_3^- + H^+ \leftrightarrow CO_3^{2-} + 2H^+$$

$$PbCl_{2(s)} + CO_3^{2-} + 2H^+ \rightarrow PbCO_{3(s)} + 2HCl_{(g)}$$

$$2PbO_{(s)} + CO_3^{2-} + 2H^+ \rightarrow Pb_2O(CO_3)_{(s)} + H_2O_{(g)}$$

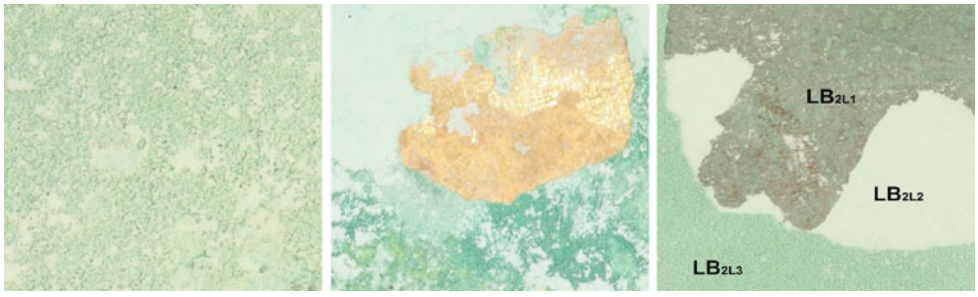

Fig. 3 Photographic documentation of the three bronzes: (**a**) TB_2, (**b**) ZB_2, and (**c**) LB_2 after the immersion in aqueous $CuCl_2$ solution for 72 h and a subsequent exposure to 100 %RH for 72 h. In (**c**) the stratification of LB_2 corrosion layers is indicated as follows: L1 corresponds to the layer adjacent to the base metal, L2 is the intermediate layer, and L3 is the external crust of LB_2

Fig. 4 SEM images of (**a**) TB_2, (**b**) ZB_2, and (**c**) LB_2, the later showing the stratification of corrosion product layers

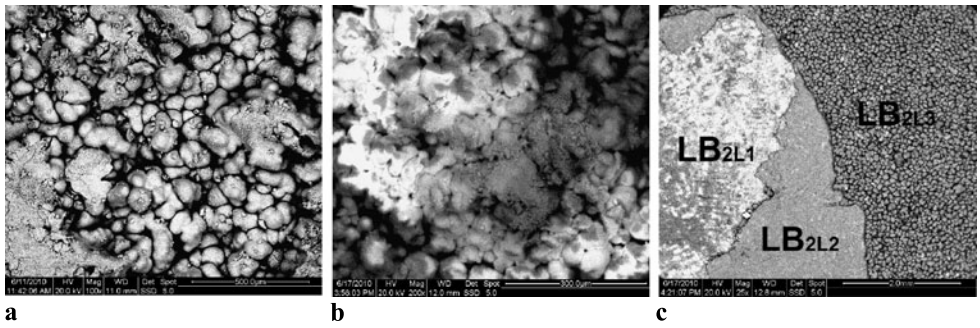

Fig. 5 Graph presenting the % molecular percentage of LB alloying elements after the exposure of LB_1 to 100 % RH, which created the corrosion layer stratification observed in LB_2. A decuprification process (Cu^{2+} migration outward) and the Pb cation mobility is evident from layer 1 toward layer 3

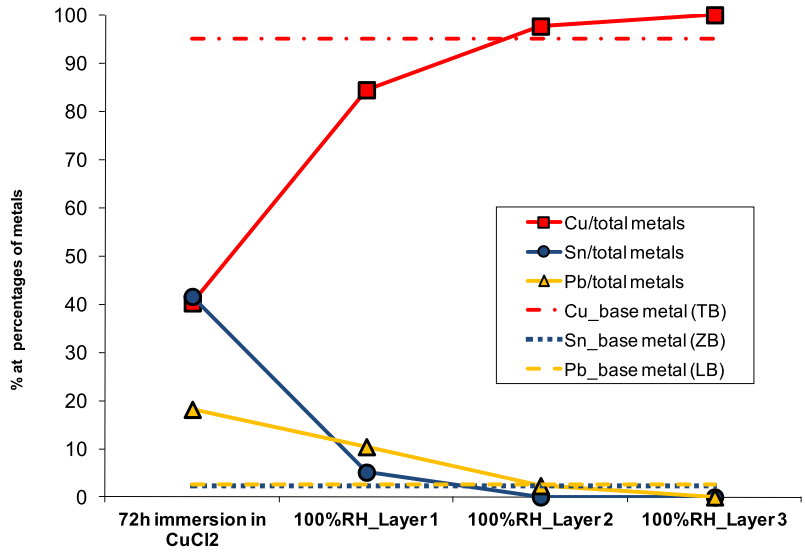

3.2 Subsequent exposure to 100 %RH conditions

After the 72 h incubation period in 100 %RH, three green, $Cu_2(OH)_3Cl$-rich patinas with different texture and morphology were created (Figs. 3 and 4). Among the three, the TB_2 patina is the thickest, has a more powdery texture, and exhibits the best adhesion to the alloy substrate. ZB_2 appears more compact but has poor adhesion. EDS (Table 2) and XRD reveal the same chemical composition for these patinas, where $Cu_2(OH)_3Cl$ predominate. On sample LB_2, three distinct corrosion layers with different colors and texture can be observed (Fig. 3c) due to partial detachment of the external crust after drying. This stratification is the result of a gradual selective diffusion of copper, i.e., decuprification process [21–23], through the passive layer created during the first corrosion stage.

This diffusion profile is depicted in Fig. 5. On the dark green layer adjacent to the base metal (LB_{2L1}), the atomic percentages of the alloying elements indicate an extensive

Fig. 6 Photographic documentation of specimens (**a**) TB_2, (**b**) ZB_2, and (**c**) LB_2 after 3 h of HGDP treatment

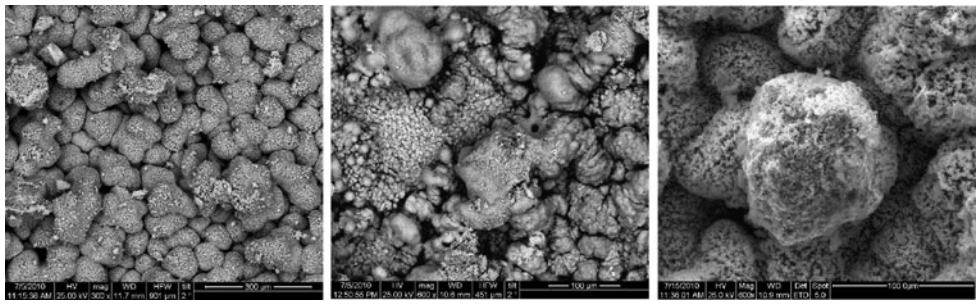

Fig. 7 SEM backscattered electron images of specimens (**a**) TB_2, (**b**) ZB_2, and (**c**) LB_2 after 3 h of HGDP

enrichment in Pb and a noticeable enrichment in Sn as compared to the initial alloy composition. XRD analysis on this layer testifies the presence of CuCl (nantokite) and $PbCl_2$. These compounds, formed during the first corrosion stage in the solution, have probably not reacted completely to $Cu_2(OH)_3Cl$ due to insufficient supply of H_2O and O_2 to the barrier film–alloy interface. In the light green intermediate layer (LB_{2L2}) the concentration of copper and chlorides rises, compared to the previous layer, tin is not detected, and the percentage of lead exhibits a slight reduction (2.3 % as compared to 2.7 % in base metal). The values of the Cl to O and Cl to Cu atomic ratios of the outer granular crust (LB_{2L3}) approximate the stoichiometric proportions for the $Cu_2(OH)_3Cl$ species. In this layer, neither Pb nor Sn are detected by EDS. This predominance of $Cu_2(OH)_3Cl$ is also confirmed by XRD analysis. The atomic percentage of Cu exceeds the corresponding measurements for the previous two layers and the base metal composition as well. The reactions that are believed to have occurred during this corrosion stage are:

$$2CuCl_{(s)} + O_{2(g)} + 2H_2O_{(g)} \rightarrow Cu_2(OH)_3Cl_{(s)} + HCl$$

$$3PbCO_{3(s)} + H_2O \rightarrow Pb_3(CO_3)_2(OH)_{2(s)} + CO_{2(g)}$$

3.3 Characterization after three hours of plasma treatment

After a three-hour HGDP treatment with hydrogen plasma the surface coloration of Sn- and Pb-bronze (TB_2 and LB_2) changed from light green to dark red (Figs. 6a and 6b). The metal regions, not covered by powdery compounds, appear black. After a few days of atmospheric exposure, though, some new light green spots appeared, indicating new outbreaks of "bronze disease."

On TB_2 XRD analysis detected metallic copper, tin and a huge quantity of nantokite as reduction products. The intensity of $Cu_2(OH)_3Cl$ peaks dropped significantly. On specimen LB_2, the reduction products are metallic copper and lead, cotunite ($PbCl_2$), and traces of nantokite (CuCl). The concentration of $Cu_2(OH)_3Cl$ species also decreased after the treatment. The morphology of the surface as revealed by SEM imaging (Figs. 7a, 7b, and 7c) does not present significant alterations.

The treatment of Zn-bronze, from the aesthetic point of view, resulted in different surface alterations (Fig. 6b). The surface acquired a golden–brown patina, and remaining blue–green regions are still visible. The acquired XRD peaks correspond to reduction products (metallic Cu and Zn) and to $Cu_2(OH)_3Cl$ compounds whose content appears reduced but still significant. The reactions occurring during the process are reduction of Cu^{2+} (present in $Cu_2(OH)_3Cl$ species) to Cu^+ and further to Cu^0 and Sn^{2+}, Zn^{2+}, and Pb^{2+} reduction to metallic Sn, Zn, and Pb, respectively. Concerning Cu, the desired chemical compound after the treatment—even more than Cu^0—is Cu_2O due to its chemical stability.

The experimental results show that Cu^+ reacts preferably with Cl than O. The explanation lies in the relative concentration of these two elements in the patina (Fig. 8). The Cl/O ratio evolution during the several steps of the experiment indicates the easier removal of O, which is in the form of hydroxides in $Cu_2(OH)_3Cl$ compounds, compared to Cl that is

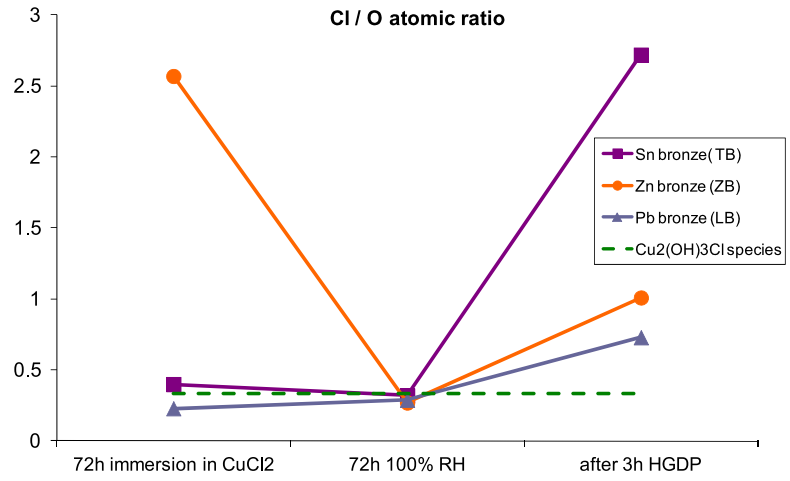

Fig. 8 Graph presenting the trend of Cl/O atomic ratio on the analyzed areas during the several steps of the experimental procedure

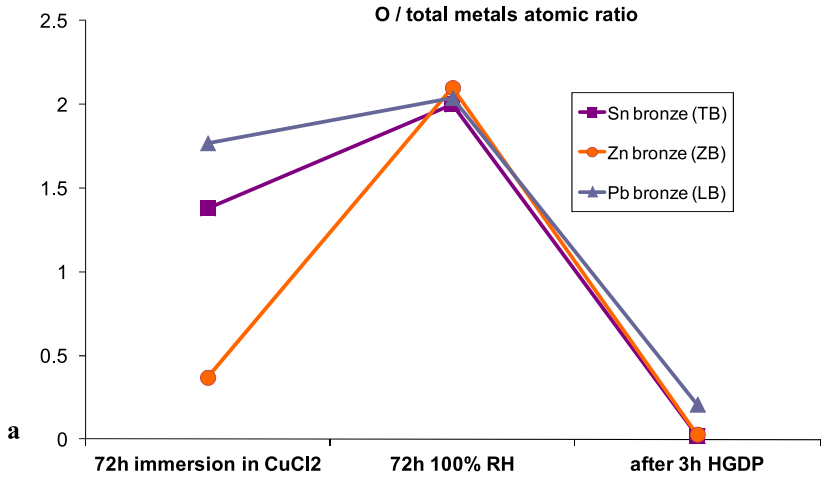

a

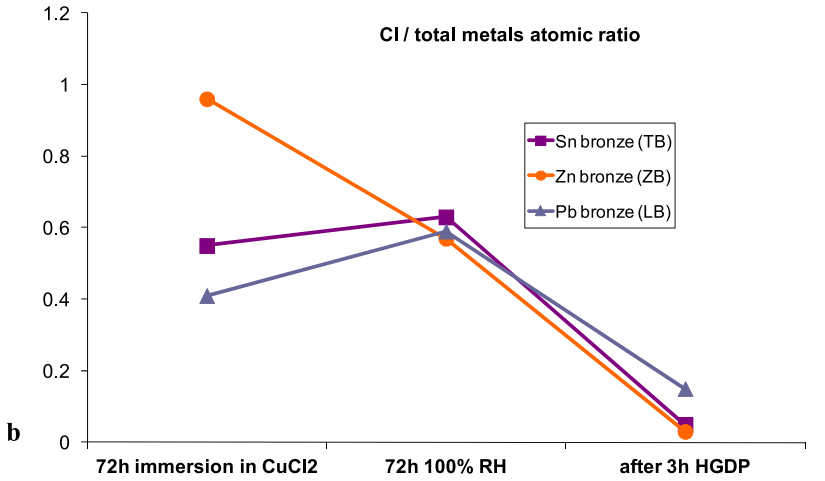

b

Fig. 9 Graphs presenting the trend of (**a**) oxygen versus total metals and (**b**) chlorine versus total metals atomic ratio on the analyzed areas during the several steps of the experimental procedure

removed with a slower rate and tends to accumulate in the form of CuCl.

Actually, the drop in the Cl molecular percentage is significant (Table 2), but the tendency for O depletion is not encouraging in terms of long-term stability of the treated surfaces. From the calculation of the atomic percentages of each metal versus total metal atoms, the enrichment in Cu of all the bronzes compared to their base metal composition is also evident (Table 3). The diminution of O and Cl content is depicted n Fig. 9.

4 Conclusions

This study highlights the impact of the various alloying elements of three different copper alloys that resemble cultural heritage marine findings to corrosion by chlorine ions, describes the chemical phenomena that arise after HGDP treatment, and evaluates the results according to the conservation requirements.

- During immersion in $CuCl_2$ solution, the Sn-bronze and even more the Pb-bronze form a corrosion layer consisting of poorly crystallized Sn and Pb compounds, which upon exposure to 100 %RH have important impact on adhesion and morphology of the synthesized $Cu_2(OH)_3Cl$ patinas.
- The Zn-bronze undergoes dezincification during immersion. Cu compounds seem to predominate over Zn, Sn, and Pb corrosion compounds, rendering the bulk metal more vulnerable to chloride attack.
- HGDP treatment achieves the removal of a great quantity of chlorides, while the surface microstructure remains mostly unchanged. This beneficial result is partly counterbalanced by the lack of sufficient oxygen in the original patinas, which becomes even less after HGDP treatment. Cu^+ species are detected as intermediate products of Cu^{2+} reduction to Cu^0. The relative concentration of chlorine compared to oxygen is high enough to favor the reaction of Cl^- with Cu^+. Thus, nantokite (CuCl) is formed instead of cuprite (Cu_2O) that would contribute to the surface stability post treatment. Nantokite cannot guarantee the specimen stability because it will react again with humidity to form $Cu_2(OH)_3Cl$.
- Surfaces after HGDP are dominated by redeposited metallic copper, while an important fraction of the chemical transformations is the reduction reactions of the rest of the alloying elements, i.e., tin, zinc, and lead.
- It should also be mentioned that the color change after the treatment would not be acceptable by some conservation protocols, especially for Sn- and Pb-bronze.

All these observations lead to the conclusion that it would be very precarious to apply HGDP on patinas with high Cl/O ratio before further optimization or additional chemical treatment that would remove the bulk quantity of chlorides.

References

1. D.A. Scott, *Copper and Bronze in Art/Corrosion, Colorants, Conservation* (Getty Publications, Los Angeles, 2002), pp. 122–134
2. I.D. MacLeod, ICCM Bull. **VII**(1), 16–26 (1981)
3. G.M. Ingo, E. Angelini, T. de Caro, G. Bultrini, I. Calliari, Appl. Phys. A, Mater. Sci. Process. **79**, 199 (2004)
4. G.M. Ingo, I. Calliari, M. Dabalà, G. Bultrini, T. de Caro, G. Chiozzini, Surf. Interface Anal. **30**, 264 (2000)
5. G.M. Ingo, E. Angelini, T. de Caro, G. Bultrini, Appl. Phys. A, Mater. Sci. Process. **79**, 171 (2004)
6. G.M. Ingo, E. Angelini, G. Bultrini, I. Calliari, M. Dabala, T. de Caro, Surf. Interface Anal. **34**, 337 (2002)
7. D.L. Hamilton, Methods of conserving underwater archaeological material culture. Conservation files: ANTH 605, Conservation of Cultural Resources. International Nautical Archaeology Program, Texas A&M University (1998). http://nautarch.tamu.edu/class/ANTH605
8. V.D. Daniels, L. Holland, M.W. Pascoe, Stud. Conserv. **24**, 85 (1979)
9. S. Veprek, J. Patscheider, J. Elmer, Plasma Chem. Plasma Process. **5**, 201 (1985)
10. S. Veprek, Ch. Eckmann, J. Elmer, Plasma Chem. Plasma Process. **8**, 445 (1988)
11. K. Schmidt-Ott, Proceedings of Metal. National Museum of Australia (2004). http://www.nma.gov.au
12. I. Kotzamanidi, E. Sarris, P. Vassiliou, C. Kollia, G.D. Kanias, G.J. Varoufakis, S.E. Filippakis, Br. Corros. J. **34**, 285 (1999)
13. I. Kotzamanidi, A. Anastasiadis, L. Filippaki, S.E. Filippakis, P. Vassiliou, E. Sarris, Anti-corros. Meth. Mater. **49**, 256 (2002)
14. Cl. Samara Ph.D. thesis. School of Chemical Engineering, National Technical University of Athens (2007)
15. J. Novakovic, O. Papadopoulou, P. Vassiliou, E. Filippaki, Y. Bassiakos, Anal. Bioanal. Chem. **395**, 2235 (2009)
16. M.P. Casaletto, T. de Caro, G.M. Ingo, C. Riccucci, Appl. Phys. A, Mater. Sci. Process. **83**, 617 (2006)
17. J.B. Sharkey, S.Z. Lewin, Am. Mineral. **56**, 179 (1971)
18. D.D. Macdonald, J. Electrochem. Soc. **139**, 3434 (1992)
19. D.D. Macdonald, M. Urquidi-Macdonald, J. Electrochem. Soc. **137**, 2395 (1990)
20. W.M. Haynes (ed.), *Handbook of Chemistry and Physics*, 69th edn. (CRC Press, Boca Raton, 1988)
21. L. Robbiola, J.M. Blengino, C. Fiaud, Corros. Sci. **40**, 2083 (1998)
22. M. Delagrammatikas, S. Diplas, O. Papadopoulou, J. Novakovic, P. Vassiliou, in *Proceedings of ECASIA 2011*, Cardiff 2011
23. M. Delagrammatikas, O. Papadopoulou, J. Novakovic, P. Vassiliou, S. Diplas, in *Proceedings of EUROCORR 2012*, Istanbul (2012)